Nonlinear dynamics of an injected quantum cascade laser

Thomas Erneux

Université Libre de Bruxelles, Optique Nonlinéaire Théorique, Campus Plaine, C. P. 231, 1050 Bruxelles, Belgium

Vassilios Kovanis

Air Force Research Laboratory, Sensors Directorate, Wright–Patterson AFB, Dayton, Ohio 45433, USA

Athanasios Gavrielides

University of New Mexico, Center for High Technology Materials, Albuquerque, New Mexico 87131-0001, USA

The stability properties of an injected quantum cascade laser are investigated analytically on the basis of current estimates of the laser parameters. We show that in addition to stable locking, Hopf bifurcations leading to pulsating intensities are possible. We discuss the stability diagrams in terms of the detuning and the injection rate for different values of the linewidth enhancement factor. The analysis indicates domains of coexistence between two stable steady states (bistability) or between a stable steady state and stable periodic oscillations. All predictions are verified numerically by determining bifurcation diagrams from the laser rate equations.

I. INTRODUCTION

Quantum cascade (QC) lasers are midinfrared semiconductor light sources based on intersubband electron transitions in coupled quantum-well systems. They are characterized by ultrafast (picosecond) carrier lifetimes, which contrast to the slow carrier lifetime of conventional semiconductor lasers (nanosecond). This property makes QC lasers ideally suited for high-speed operation. Moreover, they can be fabricated to operate anywhere between 3.5 and 20 μm, which makes them an ideal choice for infrared chemical sensing. A particular feature of QC lasers is the absence of relaxation oscillations. Relaxation oscillations are observed in most lasers used in applications (solid state, quantum well semiconductor, and CO_2 lasers) and result from the relative large carrier lifetime compared to the photon lifetime. A slight external perturbation (modulation, injection, or optical feedback) is enough to induce sustained pulsating intensities [1]. In the case of infrared chemical sensing, frequency stabilization by injection locking has been successfully used [2]. However, the possibility that a locked state may become unstable and lead to pulsating intensity regimes has never been observed experimentally.

The optically injected laser problem is the simplest experimental set-up that allows us to test the nonlinear stability of a specific laser. The dynamical possible regimes of an injected quantum well laser are well documented (see Ref. [3] for a review). More recently, the injection locking properties of vertical-cavity-surface emitting lasers [4], two-color (two-mode) lasers [5], and quantum-dot (QD) lasers [6,7] have been explored experimentally.

Most theoretical studies on the stability properties of lasers and their bifurcations are based on rate equations [1], but if we wish to determine fundamental properties of QCLs such as the gain spectra or the linewidth enhancement factor, other approaches based on microscopic kinetic equations are currently developed [8]–[10].

A recent theoretical analysis by Meng and Wang [14] concluded that the locked state of a QC laser is always stable. Wang *et al.* [15] examined the modulation properties of an injected QC laser and found instabilities for positive detunings. The main objective of this paper is to demonstrate that pulsating instabilities generated by a Hopf bifurcation are possible even for low values of the linewidth enhancement factor. To this end, we consider a minimal three-variable rate equation model. As we shall review in the next section, there is a good agreement in the literature for the values of the fixed time constants. Only the value of α remains unclear and values from −2 to 2 have been reported (see Section 3.2 in Ref. [14]). This is why analytical investigations of the injection laser problem with α as a free parameter are needed.

Specifically, we formulate the rate equations in dimensionless form and analyze the linear stability of the steady states. We show that two distinct Hopf bifurcations appear at the edges of the locking domain for a zero linewidth enhancement factor ($\alpha = 0$). Both Hopf bifurcations then progressively invade the locking domain as α is increased from zero. Above a critical value of α, one of the two Hopf bifurcations passes through the zero detuning line, limiting the locking domain to low injection rates.

The plan of the paper is as follows. In Sec. II, we formulate the rate equations and review parameter values from several references. We then carefully formulate dimensionless rate equations that are the basis of our analysis. The values of the dimensionless parameters motivate the adiabatic elimination of one of the carrier variables. The reduced equations are analyzed in Sec. III. Expressions for the stability boundaries in the detuning versus injection rate space are derived and their predictions are verified by determining numerical bifurcation diagrams in Sec. IV. Our main results are summarized and discussed in Sec. V. Mathematical details on the dimensionless formulation and on the linear stability analysis are relegated in Appendix A and B, respectively.

TABLE I. Values of the time constants (all in ps).

Parameter	Symbol	[11]	[13]	[14]	[15]
Photon lifetime	τ_p	5.77	3.7	27.6/9.91	1
Photon scatt. time $(3 \rightarrow 2)$	τ_{32}	2.1	2	1.77/0.66	1.5
Photon scatt. time $(3 \rightarrow 1)$	τ_{31}	2.6	2.44	∞	∞
Photon scatt. time $(2 \rightarrow 1)$	τ_{21}	0.3	0.3	0.26/0.14	0.21/1.2
$\tau_3^{-1} = \tau_{31}^{-1} + \tau_{32}^{-1}$	τ_3	1.16	1.1	$\tau_3 = \tau_{32}$	$\tau_3 = \tau_{32}$

II. FORMULATION

We consider the rate equations formulated by Gensty *et al.* [11] and Gensty and Elsäßer [12]. The active region of a QC laser consists of a period of N_p cascaded gain stages ($N_p = 25 - 35$). Each gain stage incorporates three energy levels labeled 1, 2, and 3 (see Fig. 1 in Ref. [12]). The carriers are injected into level 3, i.e., the upper laser level, by resonant tunneling. After the radiative laser transition $(3 \rightarrow 2)$, the carriers relax into level 1 by the emission of a longitudinal-optical phonon $(2 \rightarrow 1)$ and tunnel through the exit barrier into the subsequent miniband. For a QC laser incorporating N_p cascaded gain stages, the total number of rate equations equals $4N_p$. But under reasonable assumptions, we may reduce these equations to the following equations for the carrier populations N_2 and N_3, corresponding the energy level 2 and 3, respectively, and the total photon number within the laser cavity S

$$\frac{dN_3}{dt} = \frac{I_{\text{in}}}{q} - \frac{N_3}{\tau_{32}} - \frac{N_3}{\tau_{31}} - g(N_3 - N_2)S, \quad (1)$$

$$\frac{dN_2}{dt} = \frac{N_3}{\tau_{32}} - \frac{N_2}{\tau_{21}} + g(N_3 - N_2)S, \quad (2)$$

$$\frac{dS}{dt} = \left[N_p g(N_3 - N_2) - \frac{1}{\tau_p} \right] S. \quad (3)$$

In Eqs. (1)–(3), I_{in} is the injected current into level 3, q is the electron charge, and g is the gain coefficient. The phonon scattering times between level 3 and level 2, between level 3 and level 1, and between level 2 and level 1 are denoted by τ_{32}, τ_{31}, and τ_{21}, respectively. τ_p is the photon lifetime [11,12]. Typical values of the time constants are documented in Table I. Equations (1)–(3) are the same as the equations investigated by Petitjean *et al.* [13] with $\tau_3 \equiv (\tau_{32}^{-1} + \tau_{31}^{-1})^{-1}$ and $\tau_2 \equiv \tau_{21}$.

Supplemented by the contribution of the injected signal, the rate equations for the slave laser are given by $[E_{\text{inj}} = \sqrt{S_i} \exp(i\omega_i t), E_{\text{slave}} = \sqrt{S} \exp(i\phi) \exp(i\omega t)$, where $\omega \equiv \omega_i - \omega_0$ is the frequency detuning between master and slave lasers]

$$\frac{dN_3}{dt} = \frac{I_{\text{in}}}{q} - \left(\frac{1}{\tau_{32}} + \frac{1}{\tau_{31}} \right) N_3 - g(N_3 - N_2)S, \quad (4)$$

$$\frac{dN_2}{dt} = \frac{N_3}{\tau_{32}} - \frac{N_2}{\tau_{21}} + g(N_3 - N_2)S, \quad (5)$$

$$\frac{dS}{dt} = \left[N_p g(N_3 - N_2) - \frac{1}{\tau_p} \right] S + 2\eta \sqrt{S_i S} \cos(\phi), \quad (6)$$

$$\frac{d\phi}{dt} = \frac{\alpha}{2} \left[N_p g(N_3 - N_2) - \frac{1}{\tau_p} \right] - \omega - \eta \sqrt{\frac{S_i}{S}} \sin(\phi). \quad (7)$$

$\eta \sqrt{S_i}$ measures the amplitude of the injected field and α is defined as the linewidth enhancement factor. These equations are the same as the equations studied by Meng *et al.* [14] and Wang *et al.* [15] with $\tau_{31}^{-1} = 0$. The α parameter describes the coupling between the gain and the refractive index. For conventional diode lasers, α is typically 3–6 and arises because the two bands involved in the laser transition have opposite curvature in k space, resulting in a spectrally asymmetric differential gain. For QC lasers, the two laser subbands are within the conduction band and exhibit the same reciprocal space curvature. Consequently, QC lasers should display a symmetric differential gain and a zero α [16]. However, experiments determined nonzero values going from $\alpha = 0$ to $\alpha = 2$ [17]–[20].

In order to determine the solutions of Eqs. (4)–(7), we reformulate these equations in dimensionless form. This reformulation is essential for the success of our analysis and we detail the different steps in Appendix A. The dimensionless evolution equations exhibit a reduced number of parameters compared to Eqs. (4)–(7) and are given by

$$\frac{dZ}{ds} = \gamma_1 [P + \gamma_3 V - \gamma_4 Z - (1 + 2Z)Y], \quad (8)$$

$$\frac{dV}{ds} = \gamma_2 [2Z - V + (1 + 2Z)Y], \quad (9)$$

$$\frac{dY}{ds} = 2YZ + 2\gamma \sqrt{Y} \cos(\phi), \quad (10)$$

$$\frac{d\phi}{ds} = \alpha Z - \Omega - \gamma \sqrt{\frac{1}{Y}} \sin(\phi), \quad (11)$$

where s is time measured in units of the photon lifetime ($s \equiv t/\tau_p$). The parameters γ_1, γ_2, γ_3, γ_4, P, γ, and Ω are defined by

$$\gamma_1 = \frac{\tau_p}{\tau_{32}}, \quad \gamma_2 = \left(\frac{\tau_{32}}{\tau_{21}} - 1 \right) \frac{\tau_p}{\tau_{32}},$$

$$\gamma_3 = \left(\frac{\tau_{32}}{2\tau_{21}} - 1 - \frac{\tau_{32}}{2\tau_{31}} \right) \frac{1}{\left(\frac{\tau_{32}}{\tau_{21}} - 1 \right)},$$

$$\gamma_4 = 2 \left(1 + \frac{\tau_{32}}{2\tau_{31}} \right), \quad P \equiv \frac{N_p g \tau_p \tau_{32}}{2} \frac{I_{\text{in}} - I_{\text{th}}}{q},$$

$$\gamma = \eta \tau_p \sqrt{Y_i}, \quad \text{and} \quad \Omega = \omega \tau_p. \quad (12)$$

Using Table I, we may determine their values (see Table II). Note the relatively large values of γ_2 (underlined in Table II) compared to γ_1, γ_3, and γ_4.

TABLE II. Dimenionless parameters.

	[11]	[13]	[14]	[15]
γ_1	2.75	1.85	15.59/15.02	0.67/0.67
γ_2	<u>16.49</u>	<u>10.48</u>	<u>90.56/55.77</u>	4.1/0.17
γ_3	0.35	0.34	0.41/0.37	0.42/ − 1.5
γ_4	2.81	2.82	2/2	2/2

III. FAST ESCAPE OF CARRIERS AT THE LOWER LEVEL 2

The large value of γ_2 (see Table II) suggests to eliminate V by a quasisteady state approximation. In the limit $\tau_p/\tau_{21} \to \infty$, we first note from Eq. (12) that

$$\gamma_3 \to \frac{1}{2} \quad \text{and} \quad P \to \left(1 + \frac{\tau_{32}}{\tau_{31}}\right)\frac{(I - I_{\text{th}})}{2I_{\text{th}}}. \quad (13)$$

Eliminating then V adiabatically from Eq. (9) gives

$$V = 2Z + (1 + 2Z)Y. \quad (14)$$

Inserting Eq. (14) into the remaining equations, we obtain

$$\frac{dZ}{ds} = \gamma_1\left[P - \gamma_{41}Z - (1 + 2Z)\frac{Y}{2}\right], \quad (15)$$

$$\frac{dY}{ds} = 2ZY + 2\eta\sqrt{Y}\cos(\phi), \quad (16)$$

$$\frac{d\phi}{ds} = \alpha Z - \Omega - \eta\sqrt{\frac{1}{Y}}\sin(\phi), \quad (17)$$

where $\gamma_{41} \equiv \gamma_4 - 1 = 1.8$ for the first two columns in Table II. For the next two columns in Table II, $\gamma_{41} = 1$ and we recover the traditional semiconductor laser rate equations. By introducing $\gamma_{41} = 1$ and $Y = 2R^2$ into Eqs. (15)–(17), we find

$$\frac{dZ}{ds} = \gamma_1[P - Z - (1 + 2Z)R^2], \quad (18)$$

$$\frac{dR}{ds} = ZR + \eta_1\cos(\phi), \quad (19)$$

$$\frac{d\phi}{ds} = \alpha Z - \Omega - \frac{\eta_1}{R}\sin(\phi), \quad (20)$$

which are the dimensionless rate equations for a quantum well semiconductor laser with $\eta_1 \equiv \eta/\sqrt{2}$ [1]. There is, however, an important difference between Eqs. (18)–(20) and the rate equations of a conventional diode laser. Here, γ_1 is an $O(1)$ quantity, while γ_1 is $O(10^{-3})$ small for the conventional semiconductor laser. Provided $\gamma_1 > 8P(1 + 2P)^{-2}$, we have verified that the solitary laser ($\eta_1 = 0$) admits no relaxation oscillations. It is also worthwhile to stress that Eqs. (18)–(20) are not the equations for a Class A injected laser. For a Class A laser (such as He-Ne and Ar$^+$ lasers), the carrier Z is adiabatically eliminated and $\alpha = 0$ [1]. Equations (18)–(20) then reduce to Eqs. (19) and (20) with

$$Z = \frac{P - R^2}{1 + 2R^2}. \quad (21)$$

This reduced model (with α) was studied by Mayol *et al.* [21]. Motivated by recent work on injected locked quantum dot lasers [6,7], Eqs. (18)–(20) were recently analyzed by Kelleher *et al.* [24]

We now propose to analyze the linear stability of the steady state. As we shall demonstrate, it is possible to obtain analytical solutions in parametric form. The procedure is similar to the analysis detailed in Ref. [26] for quantum well semiconductor lasers and in Refs. [6,7] for quantum dot lasers.

From Eqs. (15)–(17), we determine the steady-state solutions for Y and Z as a function of η. The solution in parametric form is (Z is the parameter)

$$Y = \frac{2(P - \gamma_{41}Z)}{1 + 2Z}, \quad (22)$$

$$\eta^2 = [Z^2 + (\alpha Z - \Omega)^2]\frac{2(P - \gamma_{41}Z)}{1 + 2Z}. \quad (23)$$

From the linearized equations (see Appendix B), we eliminate the trigonometric functions of ϕ by using the steady-state equations. We then determine the following characteristic equation:

$$\lambda^3 - T_1\lambda^2 + T_2\lambda - T_3 = 0, \quad (24)$$

where

$$T_1 = 2Z - \gamma_1(\gamma_{41} + Y), \quad (25)$$

$$T_2 = -2\gamma_1(\gamma_{41} + Y)Z + \gamma_1(\gamma_{41} + 2Z)Y + Z^2 + (\alpha Z - \Omega)^2, \quad (26)$$

$$T_3 = -\gamma_1(\gamma_{41} + Y)[Z^2 + (\alpha Z - \Omega)^2] + \gamma_1(\gamma_{41} + 2Z)\begin{bmatrix} YZ \\ +\alpha(\alpha Z - \Omega)Y \end{bmatrix}. \quad (27)$$

We next eliminate Y using Eq. (22). The coefficients of the characteristic equation then only depend on the steady state value of Z.

We wish to determine the stability diagram in terms of the injection rate and detuning. There are two neutral stability boundaries that delimit the regions of a stable steady state. First the locking condition (saddle-node bifurcation with one zero root) and second the Hopf bifurcation condition (two purely imaginary roots). The first case implies $T_3 = 0$, or equivalently,

$$-\frac{\gamma_{41} + 2P}{1 + 2Z}[Z^2 + (\alpha Z - \Omega)^2] + 2(P - \gamma_{41}Z)[Z + \alpha(\alpha Z - \Omega)] = 0. \quad (28)$$

The second case implies $T_1T_2 - T_3 = 0$ and $T_2 > 0$. After simplifying $T_1T_2 - T_3 = 0$, we find

$$2Z\left[-2\gamma_1\frac{\gamma_{41} + 2P}{1 + 2Z}Z + Z^2 + (\alpha Z - \Omega)^2\right] - 2\gamma_1^2\frac{\gamma_{41} + 2P}{1 + 2Z}\left[-\frac{\gamma_{41} + 2P}{1 + 2Z}Z + P - \gamma_{41}Z\right] - \gamma_1 2(P - \gamma_{41}Z)[-Z + \alpha(\alpha Z - \Omega)] = 0. \quad (29)$$

The second Hopf condition $T_2 > 0$ requires the inequality

$$-2\gamma_1\frac{\gamma_{41} + 2P}{1 + 2Z}Z + \gamma_1 2(P - \gamma_{41}Z) + Z^2 + (\alpha Z - \Omega)^2 > 0. \quad (30)$$

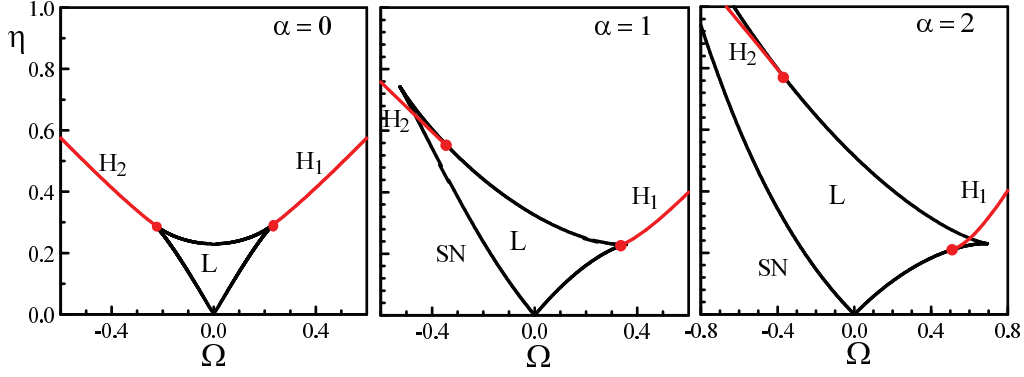The solution of these equations exists in parametric form (Z is the parameter). Changing gradually Z ($-1/2 < Z <$

FIG. 1. (Color online) Stability diagram for $P = 1$, $\gamma_1 = 2.5$, and $\gamma_{41} \equiv 1.81$. The line SN (black) delimits the domain L of steady-state locking through a saddle-node bifurcation (SN). H_1 and H_2 denote Hopf bifurcation lines (red) emerging from the SN line at Bogdanov-Takens bifurcation points (dots). From left to right, the value of α is changed from 0 to 2. The domain of stable locked steady states is bounded by the SN and Hopf lines.

P/γ_{41}), we determine $(\alpha Z - \Omega)$ from the quadratic Eqs. (28) and (29). In this way we obtain Ω as a function of Z. From Eq. (23), we then determine η as a function of Z. Three stability diagrams are shown in Fig. 1 for three different values of α. If $\alpha = 0$, the stability diagram is symmetric with respect to the $\Omega = 0$ axis and two Hopf bifurcation lines emerge from the edges of the locking domain. This diagram is similar to the one for an injected Class A laser (see Fig. 2 in Ref. [21]). As soon as α increases, the locking domain becomes asymmetric and the Hopf bifurcation lines are moving inside the domain. The one that appears for positive detuning (H_1) is responsible for a change of stability of the locked steady state as we progressively increase the detuning from a low positive value (injection rate fixed). Similarly, the second Hopf bifurcation (H_2) marks a change of stability of a steady state as we decrease the detuning from a low negative value. As we shall show

in the next section, these two Hopf bifurcations are playing determinant roles in the bifurcation diagram of the stable steady and periodic solutions.

Both Hopf bifurcation lines in Fig. 1 emerge from the locking boundaries at Bogdanov-Takens (BT) points. They are codimension-two bifurcation points that satisfy the conditions

$$T_2 = T_3 = 0. \tag{31}$$

Using Eq. (31), we may determine a parametric solution for $\Omega(Z)$ and $\alpha(Z)$ (not shown). We find two branches of solutions corresponding to the BT points associated with either H_1 or H_2; see Fig. 2. We are now ready to answer the question how a Hopf bifurcation may appear at zero detuning ($\Omega = 0$). Figure 2 indicates that this is possible for H_2 if $\alpha > \alpha_c \simeq 4.17$. $\alpha = \alpha_c$ can be determined analytically by using Eq. (31) together with $\Omega = 0$. We find that α_c^2 is given by

$$\alpha_c^2 = 2\gamma_1(P - \gamma_{41}Z)/Z^2 - 1 \geqslant 0, \tag{32}$$

where Z is the positive root of the quadratic equation

$$-4\gamma_{41}Z^2 + (2P - 3\gamma_{41})Z + 2P = 0. \tag{33}$$

For the values of the fixed parameters P, γ_1, and γ_{41} documented in Fig. 1, we find $Z = 0.3396$ and $\alpha_c = 4.1679$.

In summary, the domain of locked steady states has a triangular shape in the injection versus detuning diagram (see Fig. 1). As the linewidth enhancement factor is increased from zero, this triangle increases in size with a larger contribution in the negative detuning region α. Two Hopf bifurcations are already present in the stability diagram for $\alpha = 0$. As α increases, they penetrate into the triangular domain of the locked steady states. These Hopf bifurcations are leading to pulsating intensity regimes, which we examine in the next section.
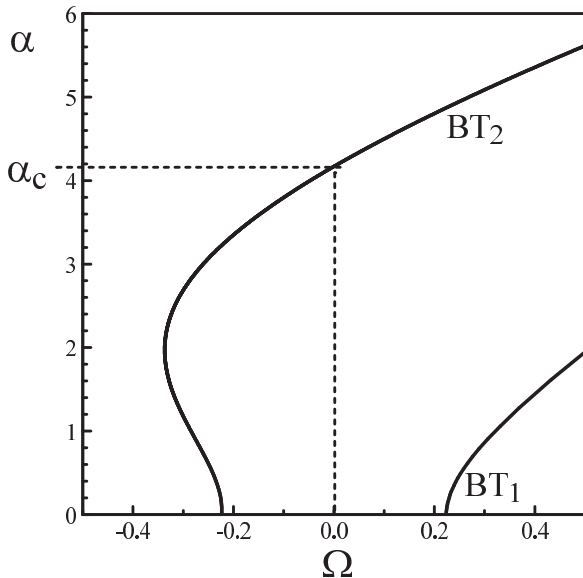

FIG. 2. Loci of the BT points in the (α, Ω) diagram. The two branches correspond to the BT points associated to the Hopf bifurcations H_1 and H_2, respectively. If $\alpha > \alpha_c$, a Hopf bifurcation H_2 is possible for $\Omega = 0$. The values of the fixed parameters P, γ_1, and γ_{41} are the same as described in the legend of Fig. 1.

IV. SIMULATIONS

If the detuning is negative, a region of steady-state bistability is possible because a Hopf bifurcation stabilizes the low-intensity steady-state branch; see Fig. 3. Simulations of Eqs. (15)–(17) have been done by increasing and then decreasing the detuning Ω in order to verify the hysteresis of the steady-state branch.
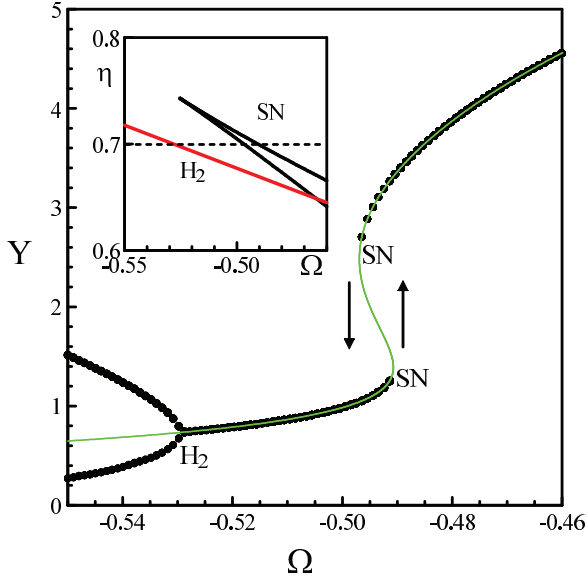
FIG. 3. (Color online) Same values of the fixed parameters as described in the legend of Fig. 1. $\alpha = 1$ and $\eta = 0.7$. The figure represents the bifurcation diagram of the extrema of Y (black dots) of the stable steady and periodic solutions. They are obtained by simulating numerically Eqs. (15)–(17). The full line (green) comes from the analytical expression of the steady state given by Eqs. (22) and (23). The inset is a blow-up of the stability diagram in the vicinity of the Hopf bifurcation (SN and Hopf lines are in black and red, respectively).

The same bistability phenomenon is possible for the conventional edge-emitting laser provided that the pump parameter is close to threshold [25] . For those lasers, experiments have been realized with a pump parameter slightly below or slightly above threshold [22,23]. As the inset in Fig. 3 indicates, the H_2 line passes one of the two SN lines as Ω passes through $\Omega = -0.46$. It allows the coexistence of stable periodic and stable steady states.

In the case of positive detuning, the Hopf bifurcation destabilizes the locked steady state as we increase the detuning from a low value of Ω see Fig. 4. A jump to large amplitude oscillations then appear as we pass the Hopf bifurcation point. Simulations of Eqs. (15)–(17) have been done by increasing and then decreasing the detuning Ω and reveal a large domain of overlap between stable steady and periodic solutions.

V. DISCUSSION

We have considered a three-variable rate equation model for a QC laser and have shown that Hopf bifurcations are possible even for low values of the linewidth enhancement factor. We also found that two locked steady states may coexist (bistability) in the negative detuning region. Furthermore, the coexistence of a stable periodic and a stable steady state is possible in the negative or positive detuning regions. This coexistence is, however, more significant in the positive detuning region.

The analysis of the Hopf bifurcation conditions was motivated by the fact that even a single mode class A laser (one single equation for the field and no relaxation oscillations) admit Hopf bifurcations if subject to an injected signal [1].
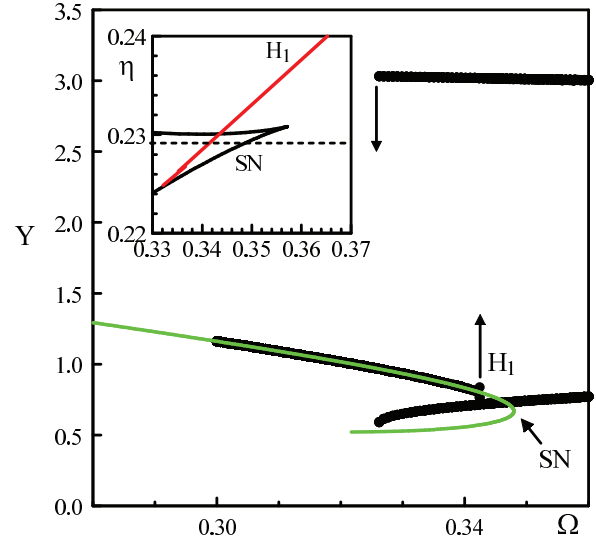

FIG. 4. (Color online) Same values of the fixed parameters as described in the legend of Fig. 1. $\alpha = 1$ and $\eta = 0.229$. The figure represents the bifurcation diagram of the extrema of Y of the stable steady and periodic solutions (black dots). They are obtained by simulating numerically Eqs. (15)–(17). The full line (green) comes from the analytical expression of the steady state given by Eqs. (22) and (23). The inset is a blow-up of the stability diagram in the vicinity of the Hopf bifurcation (SN and Hopf lines are in black and red, respectively).

The stability diagram of an injected QC laser bears striking analogies with the one of a QD laser when the latter admits strongly damped relaxation oscillations [6,7]. However, the values of the parameters appearing in the rate equations for QD lasers are not as well documented as for QC lasers. The dynamical properties of QD lasers depend on their design and fabrication, which may or may not significantly increase the damping rate of the relaxation oscillations [27].

For all our numerical simulations, we didn't find any transitions to more complex time-dependent regimes. We attribute the absence of higher-order bifurcations to the low values of α we have considered and the stronger stability of the solitary QCL compared to the conventional laser (no damped relaxation oscillations).

In order to observe the Hopf bifurcation transitions, we need sufficiently large (negative or positive) detunings of the order of 50–100 GHz. The detuning and injection strength required to observed pulsating intensities are thus a factor 10–20 larger than what is required for optically injected quantum well lasers. But this condition strongly depends on α. If $\alpha > \alpha_c \simeq 4$, we found that a Hopf bifurcation may appear in the middle of the locking domain (zero detuning).

Close to the Hopf bifurcations, the intensities exhibit oscillations with frequencies close to the Hopf bifurcation frequency $\omega_H = \sqrt{T_2} = O(1)$ where T_2 is defined by Eq. (26). The frequency in real time is then proportional to the inverse of the photon lifetime ($f_H \sim \tau_p^{-1} = 100$–200 GHz) but can be smaller if Ω is close to the BT points (see Fig. 5).

Wang *et al.* [15] investigate the case of a slow escape of the carriers at level 2. If $\tau_{21} \sim \tau_{32}$ ($\gamma_2 \sim 0$) or if $\tau_{21} \sim \tau_{32} [2(1 + \tau_{32}/\tau_{31})]^{-1}$($\gamma_3 \sim 0$), V disappears from the equation for Z. The dynamical problem then reduces to three
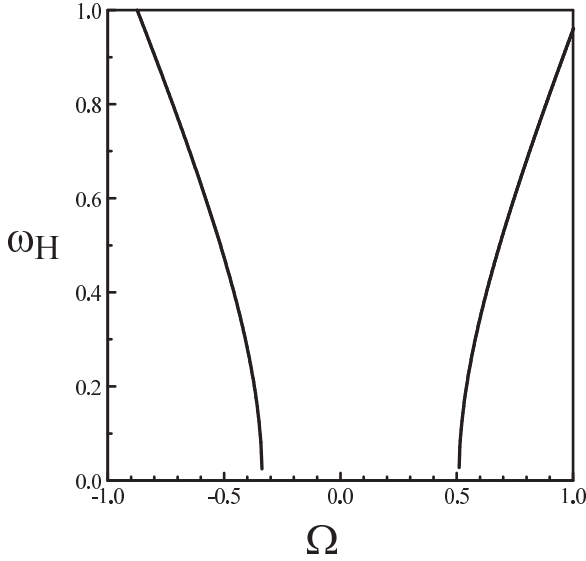
FIG. 5. Hopf bifurcation frequencies of the two Hopf bifurcation shown in Fig. 1 for $\alpha = 2$. The Hopf bifurcation frequencies $\omega_H = \sqrt{T_2}$ become zero at the BT bifurcation points.

equations for Z, Y, and ϕ. They are given by Eqs. (18)–(20) provided we rescale the intensity and three parameters ($Y \rightarrow Y/\gamma_4, \gamma_1 \rightarrow \gamma_1\gamma_4, P \rightarrow P/\gamma_4$, and $\gamma \rightarrow \gamma/\sqrt{\gamma_4}$). We found similar stability diagrams as shown in Fig. 1.

A QCL subject to optical feedback is another classical set-up for testing its stability. Experiments have been performed recently and interpreted using the Lang and Kobayachi equations modeling a conventional semiconductor laser subject to a delayed optical feedback [28]. The authors determined the first oscillatory instability (Hopf bifurcation) and explored the stabilizing effect of a large photon to carrier lifetime ratio. They also confirmed that α needs to be sufficiently large in order to destabilize the laser.

APPENDIX A: DIMENSIONLESS EQUATIONS

We consider Eqs. (4)–(7). We first introduce the new time $s \equiv t/\tau_p$ and the new variable $N \equiv N_3 - N_2$. The later is motivated by the fact that $N_3 - N_2$ appears in all four equations. We rewrite Eqs. (4)–(7) in terms of s, N, N_2, S, and ϕ and obtain

$$\frac{1}{\tau_p}\frac{dN}{ds} = \frac{I_{in}}{q} - \left(\frac{2}{\tau_{32}} + \frac{1}{\tau_{31}}\right)N$$
$$+ \left[\frac{1}{\tau_{21}} - \left(\frac{2}{\tau_{32}} + \frac{1}{\tau_{31}}\right)\right]N_2 - 2gNS, \quad \text{(A1)}$$

$$\frac{1}{\tau_p}\frac{dN_2}{ds} = \frac{N}{\tau_{32}} - \left(\frac{1}{\tau_{21}} - \frac{1}{\tau_{32}}\right)N_2 + gNS, \quad \text{(A2)}$$

$$\frac{dS}{ds} = [N_p g \tau_p N - 1]S + 2\eta\tau_p\sqrt{S_i S}\cos(\phi), \quad \text{(A3)}$$

$$\frac{d\phi}{ds} = \frac{\alpha}{2}[N_p g \tau_p N - 1] - \omega\tau_p - \eta\tau_p\sqrt{\frac{S_i}{S}}\sin(\phi). \quad \text{(A4)}$$

Second, the expression in brackets in Eqs. (A3) and (A4) motivates us to rename N so that this expression can be reduced to a single term. Specifically, we introduce the new variable Z as

$$N = \frac{1 + 2Z}{N_p g \tau_p}. \quad \text{(A5)}$$

After inserting Eq. (A5) into Eqs. (A1)–(A4), we obtain

$$\frac{2}{N_p g \tau_p}\frac{dZ}{ds} = \frac{\tau_p}{\tau_{32}}\left[\begin{array}{l}\frac{I_{in}\tau_{32}}{q} - \left(2 + \frac{\tau_{32}}{\tau_{31}}\right)\left(\frac{1+2Z}{N_p g \tau_p}\right) \\ + \left[\frac{\tau_{32}}{\tau_{21}} - \left(2 + \frac{\tau_{32}}{\tau_{31}}\right)\right]N_2 - 2g\tau_{32}\left(\frac{1+2Z}{N_p g \tau_p}\right)S\end{array}\right], \quad \text{(A6)}$$

$$\frac{dN_2}{ds} = \frac{\tau_p}{\tau_{32}}\left[\left(\frac{1+2Z}{N_p g \tau_p}\right) - \left(\frac{\tau_{32}}{\tau_{21}} - 1\right)N_2\right.$$
$$\left. + g\tau_{32}\left(\frac{1+2Z}{N_p g \tau_p}\right)S\right], \quad \text{(A7)}$$

$$\frac{dS}{ds} = 2ZS + 2\eta\tau_p\sqrt{S_i S}\cos(\phi), \quad \text{(A8)}$$

$$\frac{d\phi}{ds} = \alpha Z - \omega\tau_p - \eta\tau_p\sqrt{\frac{S_i}{S}}\sin(\phi). \quad \text{(A9)}$$

Third, the laser threshold of the solitary laser corresponds to $Z = S = 0$. From Eq. (A7) at steady state, this then implies that $N_2 = [N_p g \tau_p(\frac{\tau_{32}}{\tau_{21}} - 1)]^{-1}$. This expression motivates introducing the new variable V as

$$N_2 = \frac{1}{N_p g \tau_P}\frac{1 + V}{\left(\frac{\tau_{32}}{\tau_{21}} - 1\right)}. \quad \text{(A10)}$$

Inserting Eq. (A10) into Eqs. (A6)–(A9), we obtain

$$\frac{dZ}{ds} = \frac{\tau_p}{\tau_{32}}\left\{\begin{array}{l}\frac{N_p g \tau_p \tau_{32}}{2q}(I_{in} - I_{th}) - \left(2 + \frac{\tau_{32}}{\tau_{31}}\right)Z \\ + \left[\frac{\tau_{32}}{\tau_{21}} - \left(2 + \frac{\tau_{32}}{\tau_{31}}\right)\right]\frac{1}{2}\frac{V}{\left(\frac{\tau_{32}}{\tau_{21}} - 1\right)} - g\tau_{32}(1+2Z)S\end{array}\right\}, \quad \text{(A11)}$$

$$\frac{dV}{ds} = \frac{\tau_p}{\tau_{32}}\left(\frac{\tau_{32}}{\tau_{21}} - 1\right)[2Z - V + g\tau_{32}(1+2Z)S], \quad \text{(A12)}$$

$$\frac{dS}{ds} = 2ZS + 2\eta\tau_p\sqrt{S_i S}\cos(\phi), \quad \text{(A13)}$$

$$\frac{d\phi}{ds} = \alpha Z - \omega\tau_p - \eta\tau_p\sqrt{\frac{S_i}{S}}\sin(\phi), \quad \text{(A14)}$$

where the threshold current I_{th} satisfies the equation

$$\frac{N_p g \tau_p \tau_{32}}{2}\frac{I_{th}}{q} - \left(1 + \frac{\tau_{32}}{2\tau_{31}}\right)$$
$$+ \left(\frac{\tau_{32}}{2\tau_{21}} - 1 - \frac{\tau_{32}}{2\tau_{31}}\right)\frac{1}{\left(\frac{\tau_{32}}{\tau_{21}} - 1\right)} = 0. \quad \text{(A15)}$$

The solitary laser threshold now corresponds to $Z = S = V = 0$.

Last, we introduce the rescaled intensities Y and Y_i as

$$Y = g\tau_{32}S \quad \text{and} \quad Y_i = g\tau_{32}S_i, \tag{A16}$$

and Eqs. (A11) and (A12) reduce to Eqs. (8)–(11).

APPENDIX B: STABILITY CONDITIONS

From the linearized equations, we determine the Jacobian matrix

$$M = \begin{pmatrix} -\gamma_1(\gamma_{41} + Y) & -\gamma_1(1 + 2Z)\frac{1}{2} & 0 \\ 2Y & 2Z + \eta Y^{-1/2}\cos(\phi) & -2\eta\sqrt{Y}\sin(\phi) \\ \alpha & \frac{\eta}{2}Y^{-3/2}\sin(\phi) & -\eta\sqrt{\frac{1}{Y}}\cos(\phi) \end{pmatrix},$$

where all coefficients are evaluated at steady state. We then eliminate the trigonometric functions by using the steady-state equations and find

$$M = \begin{pmatrix} -\gamma_1(\gamma_{41} + Y) & -\gamma_1(1 + 2Z)\frac{1}{2} & 0 \\ 2Y & Z & -2(\alpha Z - \Omega)Y \\ \alpha & \frac{1}{2}Y^{-1}(\alpha Z - \Omega) & Z \end{pmatrix}.$$

We are now ready to formulate the characteristic equation for the growth rate λ. It has the form

$$\lambda^3 - T_1\lambda^2 + T_2\lambda - T_3 = 0,$$

where

$$\begin{aligned}
T_1 &= -\gamma_1(\gamma_{41} + Y) + 2Z, \\
T_2 &= -2\gamma_1(\gamma_{41} + Y)Z + \gamma_1(1 + 2Z)Y + Z^2 + (\alpha Z - \Omega)^2, \\
T_3 &= -\gamma_1(\gamma_{41} + Y)[Z^2 + (\alpha Z - \Omega)^2] + \gamma_1(1 + 2Z)Y[Z + (\alpha Z - \Omega)\alpha].
\end{aligned}$$

The stability conditions are (Routh-Hurwitz conditions)

$$T_1 < 0, \quad T_3 < 0, \quad T_1 T_2 - T_3 < 0.$$

The condition $T_1 T_2 - T_3 = 0$ is the first condition for a Hopf bifurcation. It is given by

$$\begin{aligned}
0 = {} & -\gamma_1(\gamma_{41} + Y)[-2\gamma_1(\gamma_{41} + Y)Z + \gamma_1(1 + 2Z)Y + Z^2 + (\alpha Z - \Omega)^2] \\
& + 2Z[-2\gamma_1(\gamma_{41} + Y)Z + \gamma_1(1 + 2Z)Y + Z^2 + (\alpha Z - \Omega)^2] \\
& + \gamma_1(\gamma_{41} + Y)[Z^2 + (\alpha Z - \Omega)^2] - \gamma_1(1 + 2Z)Y[Z + (\alpha Z - \Omega)\alpha],
\end{aligned} \tag{B1}$$

which can be simplified as

$$\begin{aligned}
0 = {} & -\gamma_1(\gamma_{41} + Y)[-2\gamma_1(\gamma_{41} + Y)Z + \gamma_1(1 + 2Z)Y] + 2Z[-2\gamma_1(\gamma_{41} + Y)Z + Z^2 + (\alpha Z - \Omega)^2] \\
& - \gamma_1(1 + 2Z)Y[-Z + (\alpha Z - \Omega)\alpha].
\end{aligned} \tag{B2}$$

Noting that

$$\begin{aligned}
\gamma_{41} + Y &= \frac{\gamma_{41} + 2P}{1 + 2Z} \\
(1 + 2Z)Y &= 2(P - \gamma_{41}Z),
\end{aligned}$$

Eq. (B2) can be rewritten as

$$\begin{aligned}
0 = {} & -2\gamma_1^2 \frac{\gamma_{41} + 2P}{1 + 2Z}\left[-\frac{\gamma_{41} + 2P}{1 + 2Z}Z + P - \gamma_{41}Z\right] + 2Z\left[-2\gamma_1 \frac{\gamma_{41} + 2P}{1 + 2Z}Z + Z^2 + (\alpha Z - \Omega)^2\right] \\
& - \gamma_1 2(P - \gamma_{41}Z)[-Z + (\alpha Z - \Omega)\alpha].
\end{aligned} \tag{B3}$$

The condition for a saddle-node (SN) bifurcation is $T_3 = 0$:

$$-\frac{\gamma_{41} + 2P}{1 + 2Z}[Z^2 + (\alpha Z - \Omega)^2] + 2(P - \gamma_{41}Z)[Z + (\alpha Z - \Omega)\alpha] = 0. \tag{B4}$$

[1] T. Erneux and P. Glorieux, *Laser Dynamics* (Cambridge University Press, Cambridge, UK, 2010).

[2] M. S. Taubman, T. L. Myers, B. D. Cannon, and R. M. Williams, Spectrochim. Acta, Part A **60**, 3457 (2004).

[3] S. Wieczorek, B. Krauskopf, T. B. Simpson, and D. Lenstra, Phys. Rep. **416**, 1 (2005).

[4] M. Sciamanna in *Nonlinear Laser Dynamics: from Quantum Dots to Crytography*, edited by K. Lüdge (Wiley-VCH Verlag, Berlin, 2012), Chap. 3.

[5] A. Amann in *Nonlinear Laser Dynamics: from Quantum Dots to Crytography*, edited by K. Lüdge (Wiley-VCH Verlag, Berlin, 2012), Chap. 10.

[6] T. Erneux, E. A. Viktorov, B. Kelleher, D. Goulding, S. P. Hegarty, and G. Huyet, Opt. Lett. **35**, 937 (2010).

[7] B. Kelleher, D. Goulding, S. P. Hegarty, G. Huyet, E. A. Viktorov, and T. Erneux, in *Quantum Dot Devices, Series: Lecture Notes in Nanoscale Science and Technology*, edited by M. Zhiming Wang (2012), Vol. 13, pp. 1–22.

[8] T. Schmielau and M. F. Pereira, Appl. Phys. Lett. **95**, 231111 (2009).

[9] D. O. Winge, M. Lindskog, and A. Wacker, Appl. Phys. Lett. **101**, 211113 (2012).

[10] M. S. Vitiello, R. C. Iotti, F. Rossi, L. Mahler, A. Tredicucci, H. E. Beere, D. A. Ritchie, Q. Hu, and G. Scamarcio, Appl. Phys. Lett. **100**, 091101 (2012).

[11] T. Gensty, W. Elsäßer, and C. Mann, Opt. Express **13**, 2032 (2005).

[12] T. Gensty and W. Elsäßer, Opt. Commun. **256**, 171 (2005).

[13] Y. Petitjean, F. Destic, J.-C. Mollier, and C. Sirtori, J. Select. Topics in Quant. Electr. **17**, 22 (2011).

[14] Bo Meng and Qi Jie Wang, Opt. Express **20**, 1450 (2012).

[15] C. Wang, F. Grillot, V. Kovanis, and J. Even, J. Appl. Phys. **113**, 063104 (2013).

[16] J. Faist, F. Capasso, D. L. Sivco, C. Sirtori, A. L. Hutchinson, and A. Y. Cho, Science **264**, 553 (1994).

[17] T. Aellen, R. Maulini, R. Terazzi, N. Hoyler, M. Giovannini, J. Faist, S. Blaser, and L. Hvozdara, Appl. Phys. Lett. **89**, 091121 (2006).

[18] J. von Staden, T. Gensty, W. Elsäßer, G. Giuliani, and C. Mann, Opt. Lett. **31**, 2574 (2006).

[19] M. Ishihara, T. Morimoto, S. Furuta, K. Kasahara, N. Akikusa, K. Fujita, and T. Edamura, Electron. Lett. **45**, 1168 (2009).

[20] R. P. Green, J.-H. Xu, L. Mahler, A. Tredicucci, F. Beltram, G. Giuliani, H. E. Beere, and D. A. Ritchie, Appl. Phys. Lett. **92**, 071106 (2008).

[21] C. Mayol, R. Toral, C. R. Mirasso, and M. A. Natiello, Phys. Rev. A **66**, 013808 (2002).

[22] G. H. M. van Tartwijk, H. de Waardt, B. H. Verbeek, and D. Lenstra, IEEE J. Quantum Electron. **30**, 1763 (1994); G. van Tarwijk, Ph.D. Thesis, Vrije Universiteit Amsterdam, 1994, chap. 5.

[23] A. Hohl, H. J. C. van der Linden, R. Roy, G. Goldsztein, F. Broner, and S. H. Strogatz, Phys. Rev. Lett. **74**, 2220 (1995).

[24] B. Kelleher, S. P. Hegarty, and G. Huyet, Phys. Rev. E **86**, 066206 (2012).

[25] T. Erneux, A. Gavrielides, and V. Kovanis, Quantum Semiclass. Opt. **9**, 811 (1997).

[26] A. Gavrielides, V. Kovanis, T. Erneux, Opt. Commun. **136**, 253 (1997).

[27] T. Erneux, E. A. Viktorov, and P. Mandel, Phys. Rev. A **76**, 023819 (2007).

[28] F. P. Mezzapesa, L. L. Columbo, M. Brambilla, M. Dabbicco, S. Borri, M. S. Vitiello, H. E. Beere, D. A. Ritchie, and G. Scamarcio, Opt. Express **21**, 13748 (2013).